

Characterization of nonlinear effects in a two-dimensional dielectric elastomer actuator

This article has been downloaded from IOPscience. Please scroll down to see the full text article.

2010 Smart Mater. Struct. 19 105027

(<http://iopscience.iop.org/0964-1726/19/10/105027>)

View [the table of contents for this issue](#), or go to the [journal homepage](#) for more

Download details:

IP Address: 140.114.59.160

The article was downloaded on 21/08/2012 at 05:52

Please note that [terms and conditions apply](#).

Characterization of nonlinear effects in a two-dimensional dielectric elastomer actuator

Y Jhong^{1,2}, D Mikolas¹, T Yeh², W Fang², D Shaw², J Chen² and C Fu^{1,2,3}

¹ Institute of Nano Engineering and Microsystems, National Tsing Hua University, Taiwan

No. 101, Kuang-Fu Rd., Sec. II, Hsinchu 300, Taiwan

² Department of Power Mechanical Engineering, National Tsing Hua University, Taiwan

No. 101, Kuang-Fu Rd., Sec. II, Hsinchu 300, Taiwan

E-mail: ccfu@mx.nthu.edu.tw

Received 8 February 2010

Published 15 September 2010

Online at stacks.iop.org/SMS/19/105027

Abstract

Dielectric elastomer actuators (DEAs) possess great potential for the realization of lightweight and inexpensive multiple-degrees-of-freedom (multi-DOF) biomimetic robotics. In this study, a two-dimensional DEA was built and tested in order to characterize the issues associated with the use in multi-DOF actuation. The actuator is a single circular DEA film with four, electrically isolated quadrant electrode areas. The actuator was driven in a quasi-circular manner by applying sine and cosine signals to orthogonal pairs of electrodes, and the resultant motion was recorded using image processing techniques. The effects of nonlinear voltage–strain behavior, creep and stress relaxation on the motion were all pronounced and clearly differentiated. A simple six-parameter empirical model was used and showed excellent agreement with the measured data.

(Some figures in this article are in colour only in the electronic version)

1. Introduction

Dielectric elastomer actuators (DEAs) are soft actuators capable of generating a fast response and large deformation in response to an electrical stimulus. Fast response times (below 1 ms) and recoverable strains of 380% have been reported [1, 2]. The basic configuration of DEAs consists of a dielectric film sandwiched between compliant electrodes (figure 1). Its principle of operation is that of a deformable capacitor: when applying a voltage difference across the dielectric film, the Coulomb force between free charges on the electrodes generates a net compressive stress, called Maxwell's stress, in the thickness direction. This stress, expressed as force per unit area or pressure, is given by

$$p = \epsilon_0 \epsilon \left(\frac{V}{d} \right)^2 \quad (1)$$

³ Address for correspondence: , No. 101, Kuang-fu Road, Sec. II, Hsinchu 300, Taiwan, Republic of China.

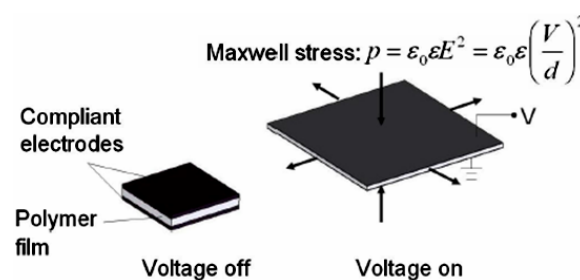


Figure 1. Principle of operation of DEAs.

where ϵ_0 is the permittivity of free space (8.85×10^{-12} F m⁻¹), ϵ is the relative permittivity of the dielectric film, V is the applied voltage and d is the thickness of the film [3].

Several types of DEAs have been proposed based on this principle. While one-dimensional actuation (elongation or contraction) is widely reported, multiple-degree-of-freedom (multi-DOF) actuations have also been realized [4–9]. For soft

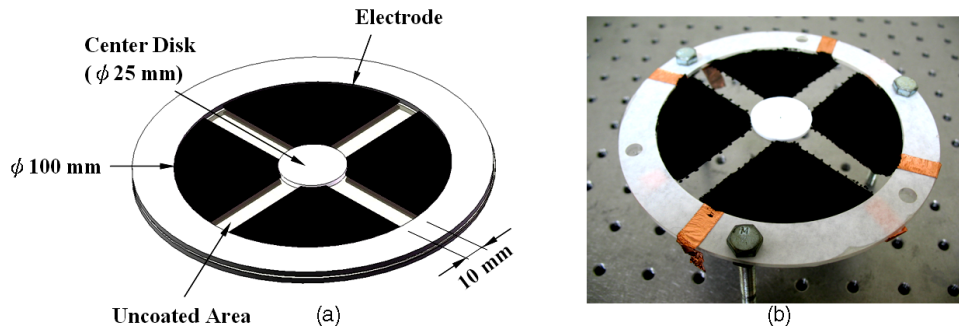


Figure 2. (a) CAD model and (b) prototype of the actuator. The black dot in the center of the center disc used for image processing has not yet been applied.

actuators like DEAs, the capability to produce actuation with multi-DOF provides a great potential in the field of lightweight, pliable and inexpensive biomimetic robotics [10]. Multi-DOF actuation from DEAs can be categorized as either localized or discrete. For localized actuation [4–7] only a single DEA element is used and multiple, electrically isolated compliant electrodes are applied to different localized regions. One can apply voltages to one or a specific set of electrodes and drive the actuator in different directions. Discrete actuators consist of one or more physically separate DEAs where each has its own, independently controlled electrodes [8, 9]. One can apply voltages to one or a specific set of actuator units to generate the desired motion.

The principle of operation of DEAs is simple, and one can design many kinds of creative actuating systems from DEAs. However, there are a number of nonlinear effects that make DEAs difficult to use in real-world applications. For example, since the force between opposite charges is always attractive, the Maxwell stress is always positive, independent of the polarity of the applied voltage. The film can only be compressed in this direction and only relax in-plane. The nonlinearity is further understood from equation (1), where we see that the stress is proportional to the square of the applied voltage divided by the square of the film's thickness.

Second, after the initial rapid actuation in response to even a constant Maxwell's stress, a further, gradual relaxation of the DEA continues. This is called polymer creep and has an approximately logarithmic behavior [11] in time, with no clear cessation even after many minutes. It is the bane of any attempt to use a simple PID algorithm to implement closed loop control.

Finally, once the externally applied stress is removed, the DEA does not completely recover its initial state. The material stores some of the applied stress. The relaxation of this internal stress happens on a timescale of the order of seconds or even minutes [12].

As mentioned above, DEAs are capable of multiple-degree-of-freedom actuation in a relatively simple manner. There is an extensive body of in-depth theoretical modeling of these and other effects in [13, 12] including direct finite element analysis [14]. However, it is still important to understand the impact of nonlinear effects beyond one dimension. In this work, we have set out to design a

test platform that will be highly sensitive to these nonlinear effects so that they can be observed and characterized. Our goal is to understand their impact on the real-world behavior of a multi-DOF actuator. We have used image processing techniques to observe two-dimensional motions of such a DEA, quantifying how the nonlinear behaviors of DEAs mentioned above—nonlinear voltage–strain behavior, polymer creep and stress relaxation—affected the trajectories of two-dimensional motions. We have chosen to use a simple empirical model which was also used and fitted with the measured data to verify our explanations about the experimental results. In this paper we consider the response of the actuator without any external loading. When DEAs are used to do real work on a load, several additional issues have been identified in the paper [15].

2. Materials and methods

2.1. Fabrication

A planar-type actuator was chosen for the simplicity of its construction and principle of operation. We chose the commercialized product VHB4910™ acrylic foam tape (3 M) as the dielectric elastomeric material since its actuating strain is substantial [15]. Moreover, it is easily accessible, inherently adhesive, uniform in physical and chemical properties, and therefore convenient for further processing. The compliant carbon grease electrodes were prepared by mixing carbon black particles with silicone oil. The proportionality between them was about 24 g/50 ml (mass of carbon/volume of oil). Electrodes were applied to each of the four quadrants of the circular film, leaving sufficient gaps to ensure electrical isolation between quadrants (figure 2). The carbon grease electrodes were applied symmetrically to both the top and bottom surfaces of the film.

Since the original thickness of the VHB4910™ film is 1 mm which is too thick for the application of DEAs, it must be prestretched biaxially. This process also offers the advantages of improving the dielectric strength and increasing the dielectric constant of the film [16]. Fixed ratio biaxial prestretch was implemented in our experiment by clamping each of the four sides of a square sample, and stretching in both directions sequentially. We limited the prestretch ratio to 3.2 by 3.2 (220% biaxial prestrain) in order to avoid tearing

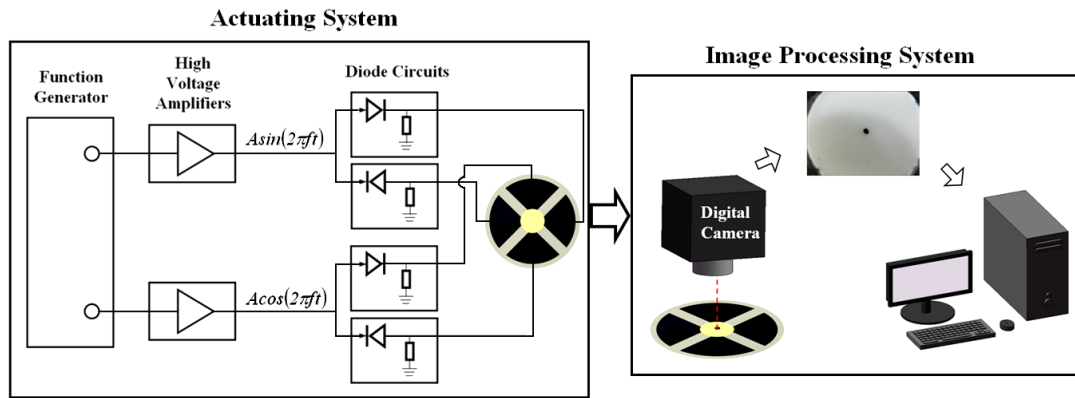


Figure 3. Experimental set-up. The actuator was driven by sinusoidal signals separated by diode circuits. The motion of the actuator (specifically, a black dot in the center of the center disc) was recorded and analyzed by an image processing system.

at the site of the clamp. Assuming that the density of the film holds constant and the film thickness is uniform everywhere after prestretching, the final thickness is about $100 \mu\text{m}$. After prestretching, the film was glued to a circular acrylic frame and then coated with carbon grease electrodes. Conductive copper foil tapes were connected to the outer edge of each of the eight electrode areas on the film (four each on the top and bottom surfaces) and served as the electrical leads. The four top electrodes received the high voltages, as shown in figure 3(a), and the bottom four electrodes were grounded. In this configuration, the center disc of the actuator can move in different directions via localized actuation. Figures 2(a) and (b) show the CAD model and prototype of the actuator, respectively.

2.2. Methods

The purpose of our measurement is to record the trajectories of two-dimensional motion of the actuator. Since circular motion is a simple starting point, we simultaneously applied sine and cosine signals to generate a two-dimensional cyclic motion. The amplitude (A) and frequency (f) of the signals were 0 to $\pm 5 \text{ kV}$ and 0.5 Hz , respectively, for 30 cycles (60 s).

We are immediately faced with the impact of the nonlinear behaviors of the DEA. The Maxwell stress is independent of the sign of the actuation voltage, so the reversal of the voltage polarity would not reverse the actuating strain. The film is always squeezed in the thickness direction, regardless of the polarity of the applied voltage. To generate a cyclic reciprocating motion, the actuator must be driven in an antagonistic manner. Positive and negative portions of the signals must be separated and then applied to opposing pairs of electrodes.

The experimental set-up is shown in figure 3. Sine and cosine signals were produced by a function generator (AFG3022, Tektronix). The amplitudes of each signal were amplified by 1000 times with two high voltage amplifiers (Model 10/10B, TREK) and then separated into their positive and negative components by four diode circuits. For each of the four channels, a series high voltage diode ($20 \text{ kV}/5 \text{ mA}$) is followed by shunt resistors ($100 \text{ M}\Omega$) to ground. The shunt

provides a load to the diode during the reverse bias period. The four amplified and filtered voltages were then applied to the actuator.

The motion of the center disc of the actuator was recorded with a digital camera and the recorded video was then analyzed with LabVIEW Vision software to acquire the position data. Video recordings of the actuator viewed from above were made with a digital camera (Canon PowerShot A630) at a rate of 30 frames s^{-1} and a resolution of 640×480 pixels. The recordings were then copied to the hard drive of a PC and were then processed using LabVIEW Vision software. For each frame, the software identified the black dot in the center of the white center disc and calculated its center in pixel space. A simple linear transform was then used to convert pixel space to real space. Separate images of a ruler were used to establish the image scaling, image rotation was aligned to the orientation of the actuator, and the origin was defined as the position of the black dot before high voltage was applied.

3. Results and discussion

3.1. Results

In our measurements, sinusoidal signals were used to generate two-dimensional, cyclic motions of the actuator. Measured results are shown in figure 4. The data points represent the positions of the center disc at different times. The origin is defined as the initial position before applying voltage. Many interesting phenomena can be observed from figure 4: first, although the signals applied to the actuator were in a simple harmonic manner, the shape of the trajectory is diamond-shaped rather than circular. Second, the enclosed area of the diamond-shaped trajectory for each cycle gradually increased as cycle number increased. Third, the orientation of the trajectory was tilted with respect to the electrode pattern. Moreover, for the clockwise rotation tests, the tilt of the diamond pattern was counterclockwise and vice versa. The inset shows the orientation of the actuator and a dotted line representing the tilt is added to guide the eye. The magnitude of the tilting was about 20° , but always in the opposite sense to the rotation.

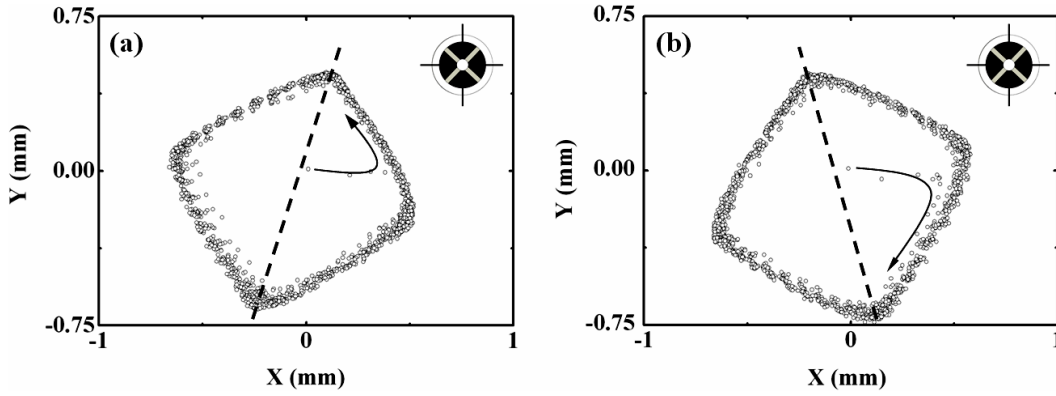


Figure 4. Trajectories of 2D cyclic motions for (a) counterclockwise and (b) clockwise rotations. ($A = 5$ kV; $f = 0.5$ Hz; $N = 30$ cycles.)

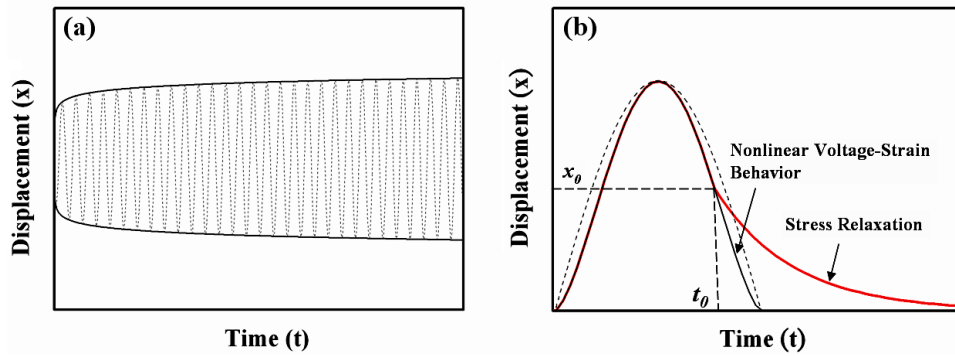


Figure 5. Time response of displacement, $x(t)$, under the effects of nonlinear behavior. (a) $x(t)$ driven by sine signal for 30 cycles influenced by creep and (b) $x(t)$ driven by sine signal (dashed line) under the influences of nonlinear voltage–strain behavior and stress relaxation.

3.2. Discussion

To explain these results, we have considered the effects of nonlinear voltage–strain behavior, creep and stress relaxation. A simple empirical model taking these nonlinear behaviors into consideration was used in order to understand their effects. The model is formulated in equation (2):

$$x(V, t) = \begin{cases} \left[1 + \gamma \text{Ln} \left(\frac{t}{\tau_{\text{creep}}} \right) \right] (c \Lambda^n), & \text{if } t < t_0 \\ x_0 e^{-t/\tau_{\text{relax}}}, & \text{if } \frac{dV}{dt} < 0 \text{ and } t \geq t_0. \end{cases} \quad (2)$$

In all, six parameters are used. The nonlinear voltage–strain behavior is parameterized as a simple power law: the displacement (x) is proportional to the power n of the dimensionless voltage ($\Lambda = V/1000$ (V)) and c is the proportional constant for the conversion to displacement. The creep and stress relaxation are both time-dependent phenomena; γ and τ_{creep} are the magnitude and characteristic time constant of the creep, and x_0 and τ_{relax} are the magnitude and characteristic time constant for stress relaxation. Creep is modeled as a slowly increasing actuation amplitude envelope for a fixed signal amplitude. A logarithmic form is typically used to fit the behavior [11]. In the case of stress relaxation,

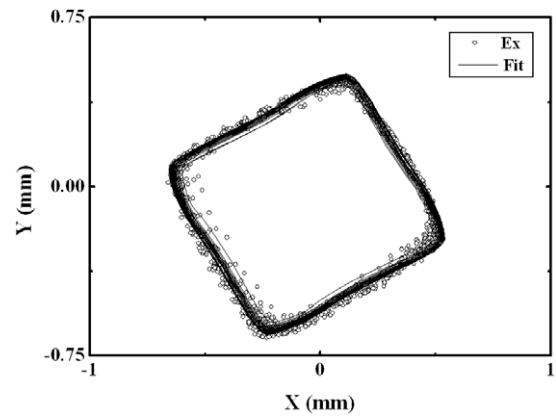


Figure 6. Empirical fit of measured trajectory in figure 5(a).

while the actuator responds promptly to an applied voltage, when the voltage is removed, at first the DEA only partially returns to its initial position. The material ‘stores’ some fraction of the stress internally. The phenomenon of stress relaxation becomes apparent when the relaxation rate is so slow that it cannot recover fast enough to keep up with the rate of decrease of the applied stress. In the model, we allow the strain to track the rising stress up to the maximum and start down the falling edge. But once a threshold level x_0 is reached (at time t_0), the strain decays exponentially as shown in figure 5(b).

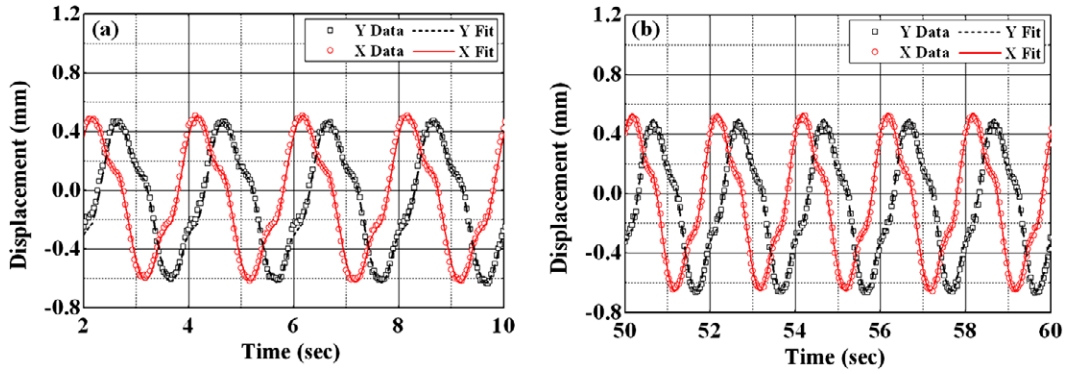


Figure 7. Empirical fit of measured data in figure 5(a) shown from (a) $t = 2\text{--}10$ s and (b) $t = 50\text{--}60$ s.

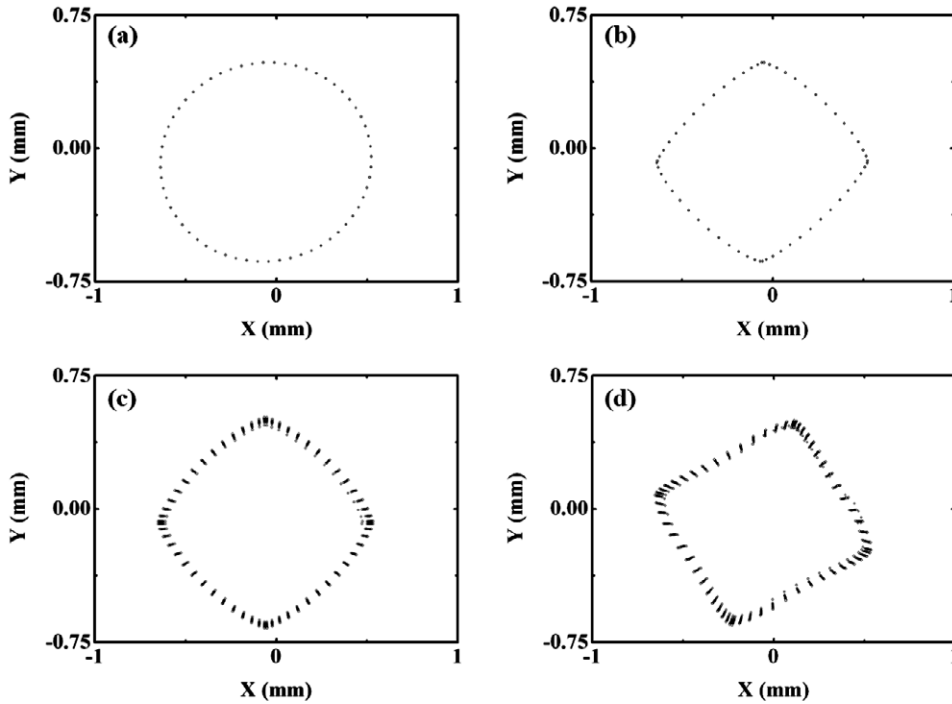


Figure 8. Simulated trajectories regarding (a) linear case ($n = 1, \gamma = 0, x_0 = 0$); (b) nonlinear voltage–strain behavior only ($n = 1.59, \gamma = 0, x_0 = 0$); (c) nonlinear voltage–strain behavior and creep ($n = 1.59, \gamma = 0.018, x_0 = 0$) and (d) nonlinear voltage–strain behavior, creep and stress relaxation ($n = 1.59, \gamma = 0.018, x_0 = 0.43$).

Whenever the actuator is started, there is always a sudden transient. This transient, or ‘hook’ denoted by the arrow in figure 4, is excluded from the fitting procedure. After the initial transient, the motion was easily fitted with the simple model without rigorous treatment. The numerical results are shown in table 1 for the fitting of figure 4(a). As shown in figures 6 and 7, the model can well describe the counterclockwise rotation. For the fitting of clockwise rotation, the numerical results were nearly the same as the counterclockwise case. The dependence of the tilt on the sense of rotation is just a consequence of swapping the up and down vertical drive voltages.

The effects of nonlinear voltage–strain behavior, creep and stress relaxation on the 2D trajectories can be discerned separately by varying the parameters accounting for each nonlinear effect. In figure 8, the parameters listed in table 1 were turned on one at a time to clearly demonstrate each of

Table 1. Empirical parameters in equation (2) accounting for nonlinear voltage–strain behavior, creep and stress relaxation. (Note: units: c and x_0 : mm, τ_{creep} and τ_{relax} : s.)

| n | c | γ | τ_{creep} | x_0 | τ_{relax} |
|------|-------|----------|-----------------------|-------|-----------------------|
| 1.59 | 0.012 | 0.018 | 1.97 | 0.43 | 0.34 |

their effects separately. When all nonlinearities were absent, as shown in figure 8(a), the model predicted the trajectory of a circle, as expected. A diamond-shaped trajectory shown in figure 8(b) was generated when only nonlinear voltage–strain behavior was considered. Under the influences of creep and nonlinear voltage–strain behavior, we can see the gradually increased enclosing area of the trajectory for each cycle in figure 8(c), and when stress relaxation was also considered, the

trajectory then tilts and sharpens as shown in figure 8(d). The results in figure 8(d) are the same as those shown in figures 6 and 7 as fitted to the experimental data.

As mentioned previously, this model has excluded the initial transient (hook) behavior and does not rigorously explain the slow drift of the center of motion away from the origin. Further study will be necessary to better understand the physical mechanisms behind them. Experiments for different signal frequencies and amplitudes are also required to see how the empirical parameters vary with different signal frequencies and amplitudes.

4. Conclusions

In this study, the two-dimensional cyclic motion of dielectric elastomer actuators (DEAs) were investigated. We have fabricated a DEA capable of performing 2D motions. The motion was generated through localized activation of electrode areas in a simple harmonic manner. We have identified at least three distinct characteristics of the motion which deviate from the expected circularity. First, we found that, under the actuation of sinusoidal voltages, the trajectory was diamond-shaped rather than circular. Second, the enclosing area of the trajectory gradually increases with time. Third, the diamond-shaped trajectory tilts relative to the orientation of the electrodes, in the direction opposite to the sense of rotation. An empirical model taking nonlinear voltage–strain behavior, creep and stress relaxation into consideration was used to fit with the experimental data. The model fits the data well and the simulated results also showed that the actual trajectory was indeed the consequence of the presence of all of these nonlinear behaviors. The model successfully describes all of these effects using six parameters to describe the material; n and c for the power-law stress–strain behavior, γ and τ_{creep} for the creep, and x_0 and τ_{relax} for stress relaxation. Other artifacts, such as the initial transient response and the slow drift of the center of motion, will require further work to be understood. Based on the success of the model, we propose that the trend of these model parameters under variation of signal amplitudes and frequencies would be informative. Much more work is needed before one can understand the whole story of the 2D motion. In short, DEAs show multiple, large, nonlinear and time-dependent effects which must be dealt with. In those potential applications of DEAs which require more than one-dimensional actuation, such as XY stages, steering mirrors and

biomimetic robotics, these studies will be necessary for the design issues of controllers, which will be critical to extract well-behaved performance.

Acknowledgments

This research was supported by the National Science Council, Taiwan for the past three years under project nos. NSC94-2218-E-007-055, NSC95-2218-E-007-024 and NSC96-2218-E-007-005. The authors would like to thank all the project team members from the National Tsing Hua University, Chang-Gung Memorial Hospital and Chaoyang University of Technology for their inspiration and involvement.

References

- [1] Pelrine R, Kornbluh R, Pei Q and Joseph J 2000 *Science* **287** 836
- [2] Zhang X, Löwe C, Wissler M, Jähne B and Kovacs G 2005 *Adv. Eng. Mater.* **7** 361
- [3] Pelrine R, Kornbluh R and Joseph J 1998 *Sensors Actuators A* **64** 77
- [4] Choi H R, Jung K M, Kwak J W, Lee S W, Kim H M, Jeon J W and Nam J D 2003 *Proc. SPIE* **5051** 262
- [5] Choi H R, Jung K M, Reyw S M, Nam J D, Jeon J W, Koo J C and Tanie K Z 2005 *IEEE-ASME Trans. Mech.* **10** 581
- [6] Bonwit N, Heim J, Rosenthal M, Duncheon C and Beavers A 2006 *Proc. SPIE* **6168** 616805
- [7] Pei Q, Rosenthal M, Stanford S, Prahlad H and Pelrine R 2004 *Smart Mater. Struct.* **13** N86
- [8] Wingert A, Lichter M D and Dubowsky S 2006 *IEEE-ASME Trans. Mech.* **11** 448
- [9] Lochmatter P and Kovacs G 2008 *Sensors Actuators A* **141** 588–97
- [10] Bar-Cohen Y (ed) 2004 *Electroactive Polymer (EAP) Actuators as Artificial Muscles: Reality, Potential, and Challenge* 2nd edn (Bellingham, WA: SPIE)
- [11] Changhai R and Lining S 2005 *Sensors Actuators A* **122** 124–30
- [12] Wissler M and Mazza E 2005 *Smart Mater. Struct.* **14** 1396–402
- [13] Yang E, Frecker M and Mockensturm E 2005 *EAPAD: Smart Structures and Materials 2005: Electroactive Polymer Actuators and Devices; Proc. SPIE* **5759** 82
- [14] Liu Y, Liu L, Zhang Z and Leng J 2009 *Smart Mater. Struct.* **18** 095024
- [15] Plante J-S and Dubowsky S 2007 *Smart Mater. Struct.* **16** S227–36
- [16] Choi H R, Jung K M, Chuc N H, Jung M Y, Koo I M, Koo J H, Lee J H, Nam J D, Cho M S and Lee Y K 2005 *Proc. SPIE* **5759** 283–91